Chemical Science

ROYAL SOCIETY OF CHEMISTRY

EDGE ARTICLE

View Article Online
View Journal

Cite this: DOI: 10.1039/d5sc09646d

All publication charges for this article have been paid for by the Royal Society of Chemistry

Near-infrared (NIR)-responsive activation of Ru-benziphthalocyanine complexes *via* singlet–triplet transition

Orie Takayama, [ab] Naoyuki Toriumi, *[a] Kenjiro Hanaoka [b] and Masanobu Uchiyama *[a]

Received 9th December 2025
Accepted 9th March 2026

DOI: 10.1039/d5sc09646d

rsc.li/chemical-science

Near-infrared (NIR) light-responsive molecules are important tools in life sciences due to high tissue transparency and low phototoxicity in this wavelength region. However, conventional compounds are generally activated *via* S_0–S_1 transition, which requires relatively high-energy excitation. Here, in order to extend the excitation wavelength into the NIR region, we designed and synthesized Ru π-arene complexes of 6π/18π tautomeric benziphthalocyanines (BPcs), aiming to utilize the low-energy singlet–triplet transition of these complexes for activation. Experimental studies revealed that selective π-coordination of Ru to the benzene ring of BPcs disrupts the strongly NIR-absorptive, 18π-electron aromatic structure of BPcs. Nevertheless, the Ru-BPc complexes still exhibit weak and broad absorption in the NIR region, derived from singlet–triplet transition with a metal-to-ligand charge-transfer character, as indicated by theoretical calculations. NIR irradiation of Ru-BPcs at >800 nm led to efficient dissociation of Ru, releasing BPcs with strong NIR absorption and fluorescence. Thus, these complexes exhibit OFF/ON-type activation *via* NIR-induced Ru release due to S_0–T_1 transition.

Introduction

Near-infrared (NIR) light, in the wavelength range from 700 to 2500 nm, is advantageous for optoelectronic applications such as security printing, sensors, and solar cells, as well as for biomedical applications such as bioimaging, and photodynamic therapy due to high tissue transparency in this wavelength range, low tissue-damaging potential, and high spatial resolution.[1–7] Among the tremendous number of NIR-absorbing organic dyes, NIR-responsive molecules that undergo chemical transformation upon NIR irradiation are particularly useful for spatiotemporal imaging and therapeutic applications. Representative examples include photoswitches and photocages, which exhibit reversible and irreversible structural changes, respectively, upon NIR photoexcitation (Fig. 1a, up).[8–10] These molecules are typically based on organic chromophores such as azobenzene, diarylethene, BODIPY, methylene blue, *etc.*, which absorb in the UV-visible to NIR region.[11–17] They commonly undergo photoreactions such as photooxidation, photolysis, photoisomerizations, and electrocyclic reactions *via* excitation from the singlet ground state (S_0) to the lowest singlet excited state (S_1).[10,17] However, while a variety of molecules and mechanisms have been reported for NIR-responsive systems, the available excitation wavelengths are often restricted to the red or shorter-wavelength NIR regions (600–750 nm) due to the relatively large energy gaps of the S_0–S_1 transitions. To fully exploit the advantages of NIR light, novel molecular designs and reaction mechanisms are required to enable efficient excitation at longer NIR wavelengths, where tissue transparency is higher and phototoxicity is lower.

To address this need, we focused on transition metal π-arene complexes, which show characteristic photoinduced ligand dissociation under UV or visible light irradiation[18–24] due to weakening of the strong interaction between the arene π-systems and metal d-orbitals upon photoexcitation (Fig. 1a, down).[21] Notably, however, lower-energy transitions from S_0 to the lowest triplet state (T_1) are also effective for arene photodissociation owing to efficient intersystem crossing in transition metal complexes.[19] We therefore hypothesized that transition metal π-complexation with NIR-activatable dyes would afford compounds with longer-wavelength NIR photoreactivity due to S–T transition.

To test this idea, we focused on benziphthalocyanines (BPcs) as a candidate molecular platform for π-complexation. BPc is a phthalocyaninoid in which one of the four isoindoline units of phthalocyanine is replaced by a benzene ring.[25,26] We have recently developed BPcs as OFF/ON switchable NIR dyes, whose NIR properties are controllable by tautomerization of the 6π ⇄ 18π aromaticity in response to external environmental factors (Fig. 1b).[27–32] Introducing one or two hydroxy groups on the

[a]Graduate School of Pharmaceutical Sciences, The University of Tokyo, 7-3-1 Hongo, Bunkyo-ku, Tokyo 113-0033, Japan. E-mail: toriumi@mol.f.u-tokyo.ac.jp; uchiyama@mol.f.u-tokyo.ac.jp

[b]Graduate School of Pharmaceutical Sciences, Keio University, 1-5-30 Shibakoen, Minato-ku, Tokyo 105-8512, Japan

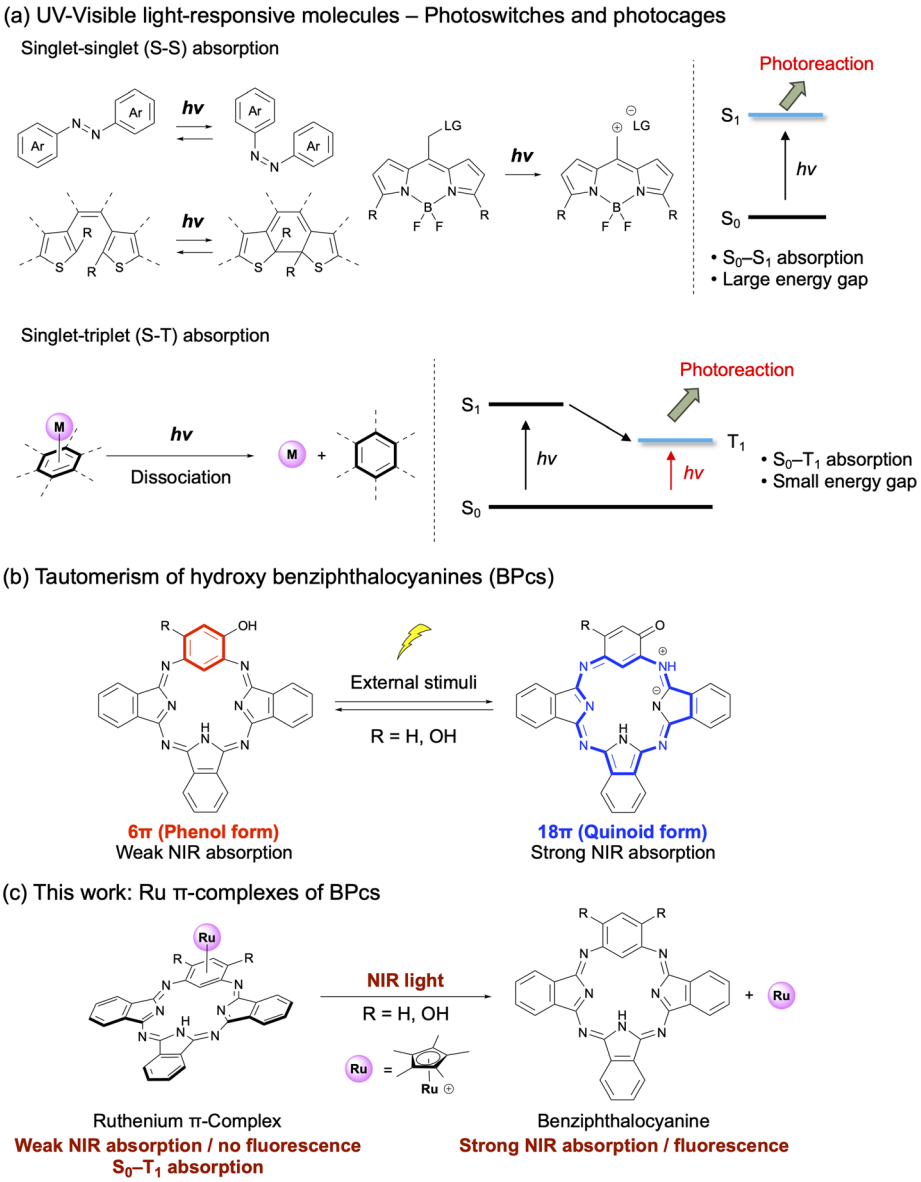

Fig. 1 Background and concept of this work. (a) Examples of UV-visible light-responsive molecules. Photoswitches and photocages based on singlet–singlet (S–S) absorption and photodissociation of transition metal π-arene complexes based on singlet–triplet (S–T) absorption. (b) Tautomerism of hydroxy benziphthalocyanines (BPcs).[27,29,30] (c) This work: NIR-responsive photodissociation and activation of Ru π-arene complexes of BPc.

benzene ring results in phenol–quinoid tautomerism. In the phenol form, 6π-electron aromaticity of the benzene unit results in cross-conjugation and weak NIR absorption of the macrocycle. On the other hand, in the quinoid form, electron donation from the hydroxy group alters the aromaticity of the benzene ring, leading to delocalized 18π-electron aromaticity and strong NIR absorption. This tautomerism was utilized to achieve reagent-, solvent-, and pH-responsive control of NIR absorption and emission.

In the present work, we designed and synthesized photoresponsive Ru π-complexes of BPc ligands with switchable aromaticity, based on the idea that π-complexation would influence the BPc tautomerism. Various transition metal π-complexes based on porphyrinoid ligands have been synthesized,[33–40] which could potentially be available for biomedical applications using NIR light. However, to our knowledge the photoresponsive (photodissociation) behavior of porphyrinoid π-metal complexes has scarcely been documented. Therefore, we synthesized a series of Ru π-complexes bearing BPc ligands with varying numbers of hydroxy groups and studied their electronic structures and photochemical properties (Fig. 1c). We found that the Ru complexes underwent decomplexation upon NIR irradiation at wavelengths >800 nm, liberating 18π aromatic BPc. Thus, these complexes enable OFF/ON control of NIR absorption and fluorescence *via* NIR-induced Ru release due to S_0–T_1 transition. We anticipate that the present detailed characterization of the Ru-BPcs platform will afford a solid foundation for future applications research.

Results and discussion

Synthesis

BPc **1** and monohydroxy BPc **2** were prepared by condensation of the appropriate 1,3-phenylenediamine and 1,3-diiminoisoindoline according to our previously reported procedures.[29,32] To obtain Ru π-complexes of BPcs, we focused on the well-known $[Cp^*Ru(\eta^6\text{-arene})]^+$ complex ($Cp^* = \eta^5\text{-}C_5Me_5$) because of the excellent stability of the Cp*Ru unit.[20] Cationic Cp*Ru-BPc complexes **3** and **4** were synthesized in 79% and 80% yields, respectively, by treating BPcs **1** and **2** with $[Cp^*Ru(MeCN)_3]PF_6$ in $CHCl_3$ at 60 °C (Fig. 2). As for **4**, Ru complexation of **2** followed by deprotonation of the phenolic proton with Na_2CO_3 aq. gave phenoxo-type neutral Cp*Ru-BPc complex **4A** (see SI).[41–43] No regioisomers or multi-coordinated by-products were detected for either **3** or **4**. Ru-BPcs **3** and **4** slowly decomposed in solution under ambient conditions (~1% and ~6% decomposition in $CDCl_3$ over 4 days for **3** and **4**, respectively), but could be stored at room temperature as stable solids for more than 3 months under an Ar atmosphere in the dark.

Single-crystal X-ray analysis was examined for the structure determination of the Ru complexes. Despite investigating various conditions, we failed to obtain crystals of **3** and **4** suitable for X-ray analysis. Instead, we synthesized cationic Cp*Ru-BPc complex **3X**, which possesses less flexible 2,6-dimethylphenoxy groups at the peripheral positions and a rigid carborane counter anion $[CB_{11}H_6Br_6]^-$ (see SI). In this case, a good crystal was obtained, and the molecular structure of **3X** in the solid state was successfully confirmed by X-ray analysis (Fig. 3). The RuCp* unit was bound to the sterically less hindered benzene unit in an η^6 fashion. The BPc skeleton was distorted and saddle-shaped due to the interaction of the BPc skeleton and the carborane anion.

Physicochemical properties

Next, to investigate the structure and aromaticity of Ru complexes **3** and **4** in solution, their ^{1}H NMR spectra were recorded in $CDCl_3$ and compared with those of BPcs **1** and **2**, respectively (Fig. 4a). The signals of Ru complex **3** were assigned with the help of ^{13}C and ^{1}H–^{13}C HSQC and HMBC measurements (Fig. S20), which indicated η^6-coordination of Ru to the benzene unit, consistent with the X-ray structure. The C–H^b, H^c, and H^d protons on the Ru-arene moiety of **3** were observed at 6.10–5.80 ppm, shifted upfield by 1.32–0.94 ppm relative to those of BPc **1**. The ^{13}C signals of the Ru-arene moiety of **3** were also shifted upfield (113–73 ppm). This tendency is typical of Ru π-arene complexes, and reflects shielding effects caused by the d electrons of Ru(II).[44] The signal of the internal N–H^a proton of **3** appeared at 11.75 ppm, differing by only 0.04 ppm from that of **1**, which indicates that complexation with Ru has little effect on the macrocyclic 18π-aromaticity. Similarly, the ^{1}H spectrum of **4** supports Ru complexation to the phenol moiety of BPc **2**. The external C–H^c and H^d protons were both observed at 5.82 ppm, shifted upfield by 1.93–1.26 ppm compared with those of BPc **2**. In contrast, the internal N–H^a and C–H^b protons were observed at 11.22 and 6.27 ppm, downfield by 1.77 and 0.11 ppm compared with those of **2**, respectively, which can be attributed to the weakened 18π-aromatic ring current effect. In other words, the electron-withdrawing cationic Cp*Ru unit shifts the phenol–quinoid tautomerism towards the phenol form. Deprotonated Ru complex **4A** exhibited upfield ^{1}H NMR chemical shifts compared with **4**, reflecting its higher electron density (see SI).

The tautomeric shift in **4** was further rationalized by DFT calculation at the M06/6-31G(d,p)-SDD(Ru) level (Fig. 4b). We used model substrates **1′**–**4′** lacking any peripheral substituents and counter anions for **1**–**4**. For BPc **2′**, the phenol form is favored by 2.87 kcal mol^{-1} over the quinoid form, suggesting

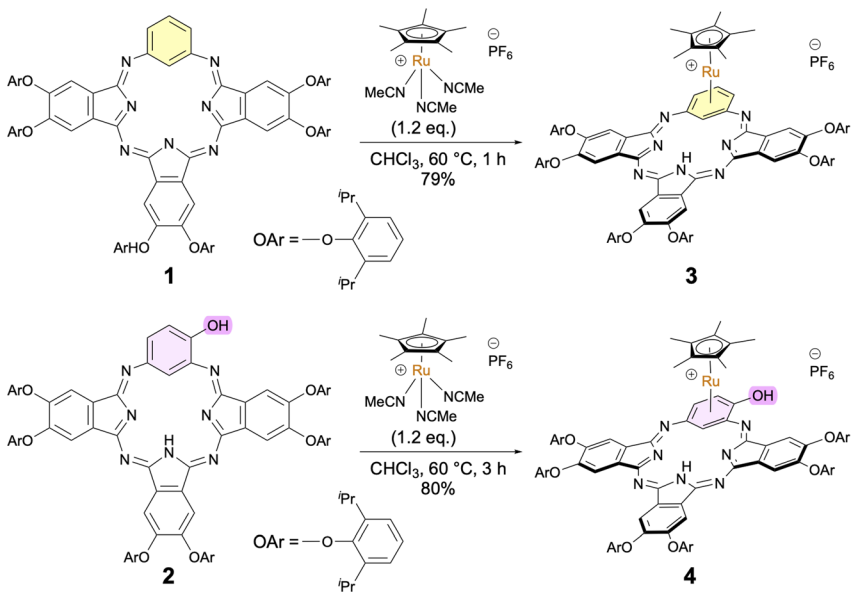

Fig. 2 Synthesis of Ru complexes **3** and **4**.

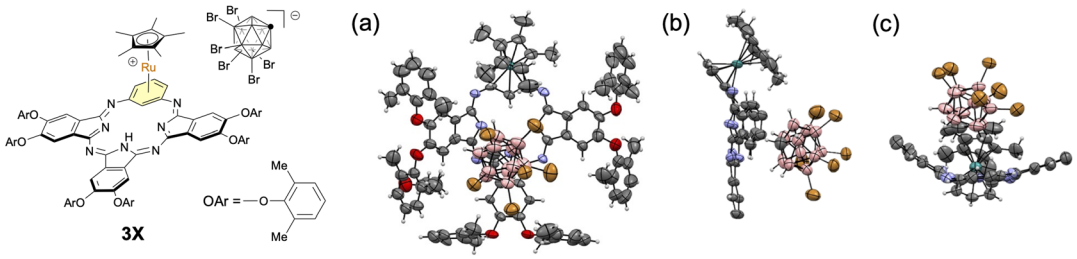

Fig. 3 Single-crystal X-ray structure of **3X**. (a) Top view. (b) Side view. (c) Bottom view. Thermal ellipsoids set at 50% probability. One of the two molecules in the asymmetric unit is shown. In (b) and (c), the 2,6-dimethylphenoxy groups are omitted for clarity.

that **2** can show tautomerism between the phenol form and the quinoid form, although the equilibrium would favor the phenol form. In contrast, the phenol form of **4′** is 8.55 kcal mol^{-1} more stable than the quinoid form of **4′**, indicating that **4** is present predominantly as the phenol form. Additionally, the nucleus-independent chemical shifts (NICS) of **2′** and **4′** in the phenol form and the quinoid form were calculated at the center of the macrocycle. The NICS(0) values indicate that **4′** has much weaker 18π-aromaticity than BPc **2′** (**2′**-phenol: −3.56 ppm; **2′**-quinoid: −10.81 ppm; **4′**-phenol: +0.27 ppm; **4′**-quinoid: −2.04 ppm), consistent with the observed ^{1}H chemical shifts. This indicates that the Ru atom accepts 6π electrons from the phenol unit, interrupting the macrocyclic 18π-aromatic conjugation pathway.

Electronic absorption spectra of **1–4** were measured in CH_2Cl_2 to evaluate the effect of π-complexation (Fig. 5a). BPc **1** and Ru complex **3** both exhibited a broad absorption band in the region of 450–600 nm. This indicates that the effect of π-coordination on the singlet–singlet (S–S) absorption is relatively small, in accordance with the small change observed in the aromatic region of the ^{1}H NMR spectra. However, it is noteworthy that the absorption tail of **3** reached 900 nm in the NIR region, which is not so in the case of **1**. We consider this broad NIR absorption is derived from S–T transition. Although direct S–T absorption is spin-forbidden in general, some transition metal complexes including Ru have large absorption coefficients ($\varepsilon > 1000$) owing to strong spin–orbit coupling.[45–47] BPc **2** exhibited a broad absorption band in the visible region with a small band at 861 nm in the NIR region, attributable to a small contribution of the quinoid form.[29] Ru complex **4** exhibited a similar spectrum to **3**, which is clearly different from that of BPc **2** with distinct absorption bands in the region of 500–700 nm. This is consistent with the weakened 18π-aromaticity that accompanies Ru complexation. Broad NIR absorption similar to that of **3** was also observed for **4**. None of the compounds **1–4** showed detectable emission at room temperature under an Ar atmosphere.

Time-dependent density functional theory (TD-DFT) calculation and molecular orbital analysis of **1′–4′** were conducted to gain further insights into the optical properties of the Ru complexes (Fig. 5b, S7–S12, and Tables S3–S8). The nodal patterns of the HOMO, HOMO−1, and LUMO of **1′** and **2′** in the phenol form can be interpreted in terms of the 18π-electron perimeter model (Fig. S7–S9).[48] In contrast, the HOMO and HOMO−1 of Ru complex **3′** are delocalized over both the BPc and Ru, and can be regarded as a combination of the HOMO and HOMO−1 of **1′** with the d orbital of Ru (Fig. 5b, left). The LUMO of **3′** is localized on the BPc with little contribution of Ru. Thus, the $S_0 \rightarrow S_1$ and $S_0 \rightarrow S_2$ transitions of **3′** ($S_0 \rightarrow S_1$: 510 nm, $f = 0.0007$; $S_0 \rightarrow S_2$: 504 nm, $f = 0.1370$) have a metal-to-ligand charge transfer (MLCT) character. The computed $S_0 \rightarrow T_1$ transition of **3′** (639 nm) also originates from the HOMO → LUMO transition and has a MLCT character, and its energy matches the observed NIR broad absorption (Table S6). **4′** was calculated to show a similar tendency to **3′** ($S_0 \rightarrow S_1$: 533 nm, $f = 0.0094$; $S_0 \rightarrow S_2$: 510 nm, $f = 0.1606$; $S_0 \rightarrow T_1$: 665 nm) (Fig. 5b, right, Table S7). The observed $S_0 \rightarrow T_1$ absorption bands ($\varepsilon \sim 1000$) are stronger than those of Pc complexes with central transition metals ($\varepsilon \sim 200$), where the admixture of π* (*e.g.*, LUMOs of Pc) and d_π orbitals is small.[49] Efficient orbital mixing between BPc and Ru through π-arene bonding presumably accounts for the intense S_0–T_1 absorption.

NIR-responsive photoreactivity

The ^{3}MLCT absorption in the NIR region prompted us to investigate the photoreactivity of the Cp*Ru-BPc complexes, since [Cp*Ru(η^6-arene)]$^+$ sandwich complexes are known to release the arene ligands in the triplet excited state.[18–21] We examined Ru dissociation of **4** to yield free BPc **2** in C_6D_6 (Fig. 6). Irradiation with NIR light ($\lambda = 740$ nm) at 20 °C for 4 h afforded BPc **2** in 14% yield (entry 1). We found that addition of coordinating ligands was effective for the Ru dissociation (Table S1); for example, AcOH accelerated the reaction under irradiation, giving BPc **2** quantitatively (entry 2). We think AcOH may act as a transient coordinative ligand to Ru in the reaction, since the dissociation of π-arene complexes is promoted by coordinating solvents or weak ligands in general,[42,50] and this could assist the environment-responsive photo-uncaging of Ru. This reaction did not occur in the dark in the absence or presence of AcOH (entries 3 and 4). Heating at 80 °C instead of NIR irradiation with AcOH promoted the reaction but the yield was low, indicating that the reaction under NIR irradiation would not be accelerated by photothermal effects (entry 5). The dissociation proceeded with 850 nm NIR light, but was not promoted by 940 nm NIR light (Table S2), consistent with the observed S_0–T_1 absorption of **4**. The generation of [Cp*Ru(η^6-C_6H_6)]PF_6 after the reaction was confirmed by using C_6H_6 instead of C_6D_6. In contrast to the NIR photoreactivity of **4**, Cp*Ru-BPc complex **3**,

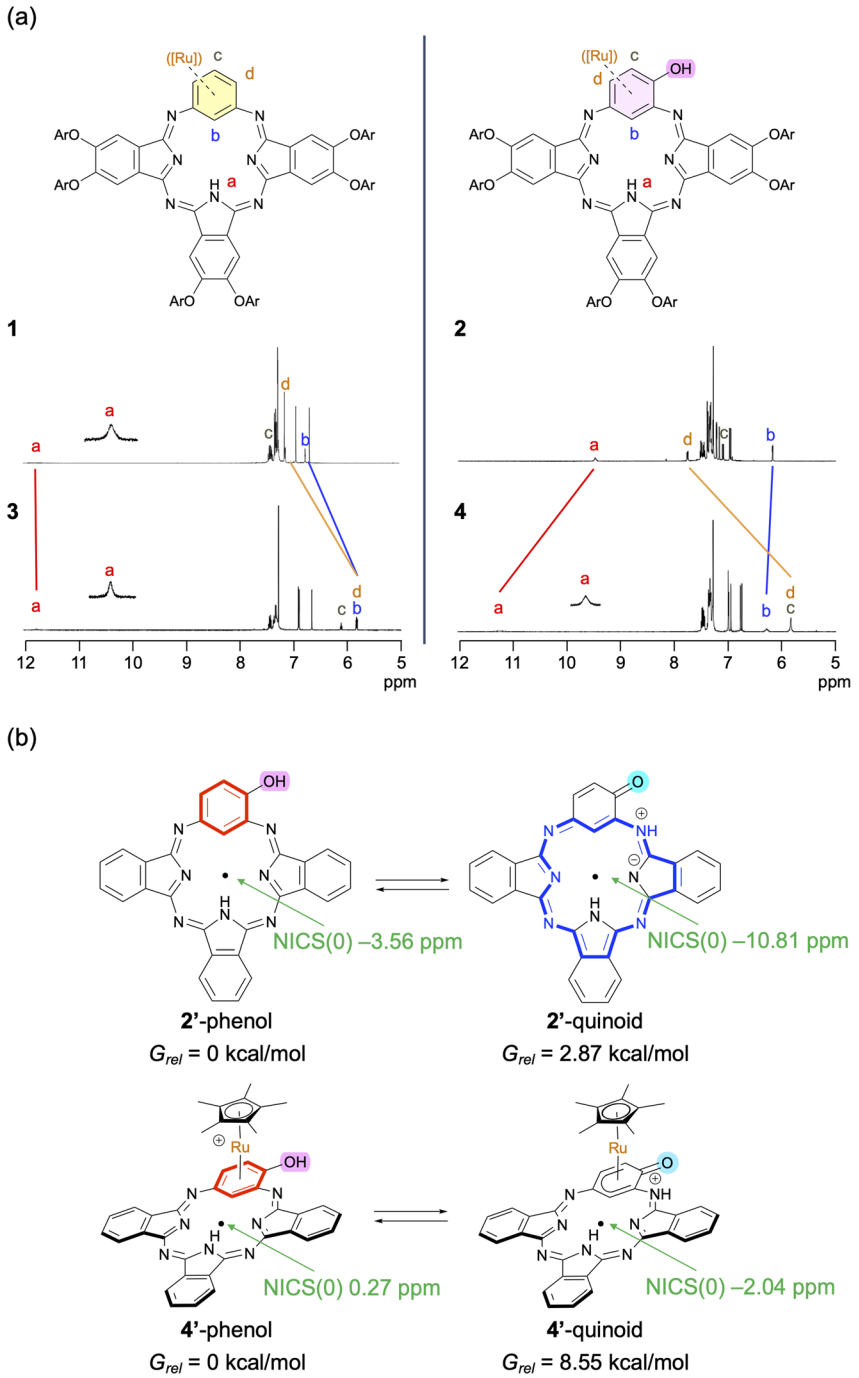

Fig. 4 Aromatic properties. (a) Partial ^{1}H NMR spectra of **1**–**4** in $CDCl_3$. (b) Calculated NICS(0) values and energy differences between the phenol and quinoid forms of **2′** and **4′**.

which lacks a hydroxy group, did not undergo Ru dissociation at all under irradiation at 740 nm in the presence of AcOH (entry 6), even though its absorption band reaches 1000 nm (Fig. 5a). Notably, the difference of the photoreactivity between **3** and **4** could not be attributed to the values of their molar absorption coefficients (ε), since the reaction of **4** proceeded even under irradiation at 850 nm ($\varepsilon = 348$), where the value of ε is similar to that of **3** at 740 nm ($\varepsilon = 416$). These findings suggest that **4** is more reactive in the arene exchange process under irradiation compared to **3**.

Importantly, the NIR excitation wavelength of 850 nm for Ru dissociation is substantially longer than those of reported Ru-based photoactive systems that rely on red or far-red light (<800 nm).[51–54] This clearly highlights the advantage of utilizing low-energy S–T transitions over conventional high-energy S–S transitions.

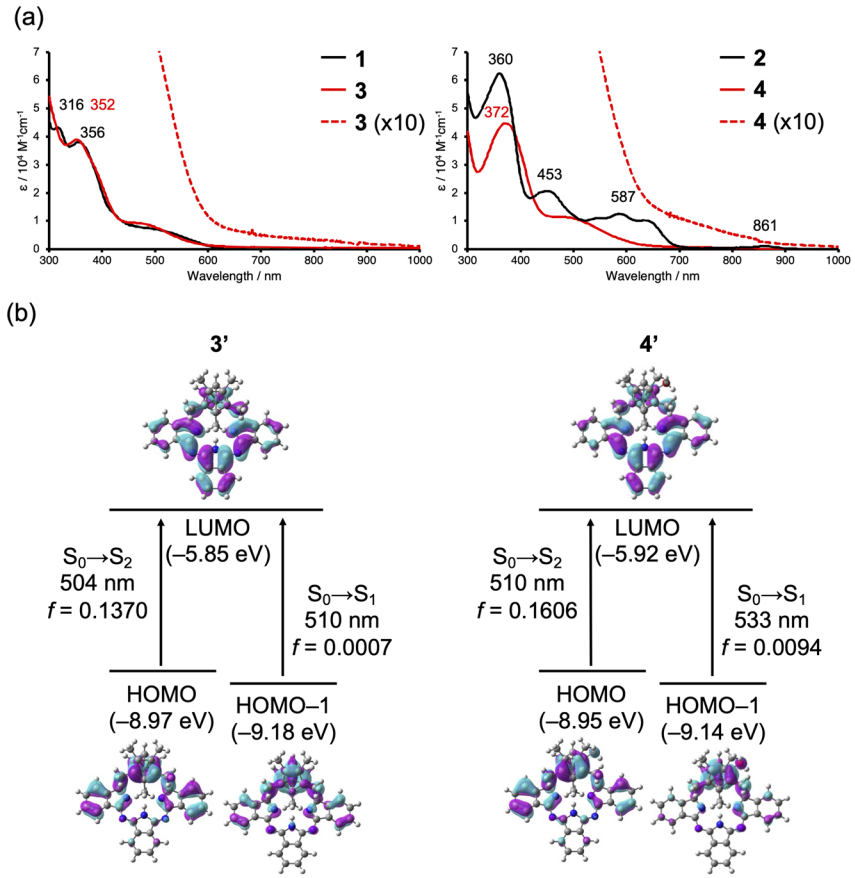

Fig. 5 Photophysical properties. (a) Electronic absorption spectra of **1** (left, black), **3** (left, red), **2** (right, black), and **4** (right, red) measured in CH_2Cl_2. (b) Major electronic transitions (TD-DFT) contributing to low energy absorptions and representative frontier molecular orbitals for Ru complexes **3′** (left) and **4′** (right).

To gain insight into the different reactivity of **3** and **4**, the thermodynamic stability in the arene exchange reaction with C_6H_6 was calculated for Ru complexes **3′** and **4′** (Fig. S6). The reactions were found to be exothermic for both **3′** and **4′** with ΔG of -8.42 kcal mol^{-1} and -12.15 kcal mol^{-1}, respectively, suggesting **4** is more stabilized by the arene exchange than **3**. This

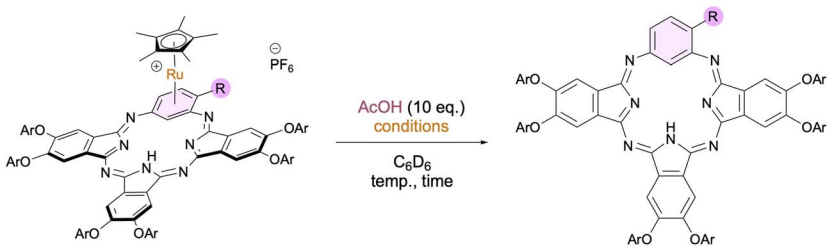

entry	substrate	AcOH	conditions	temp. (°C)	time (h)	yield (%)[a]
1	**4**	x	*hv* (740 nm)	20	4	14
2	**4**	o	*hv* (740 nm)	20	4	quant.
3	**4**	x	dark	20	24	0
4	**4**	o	dark	20	24	0
5	**4**	o	dark	80	4	21
6	**3**	o	*hv* (740 nm)	20	4	0

Fig. 6 Photochemical arene release reaction of **3** and **4**. [a]Determined by ^{1}H NMR analysis.

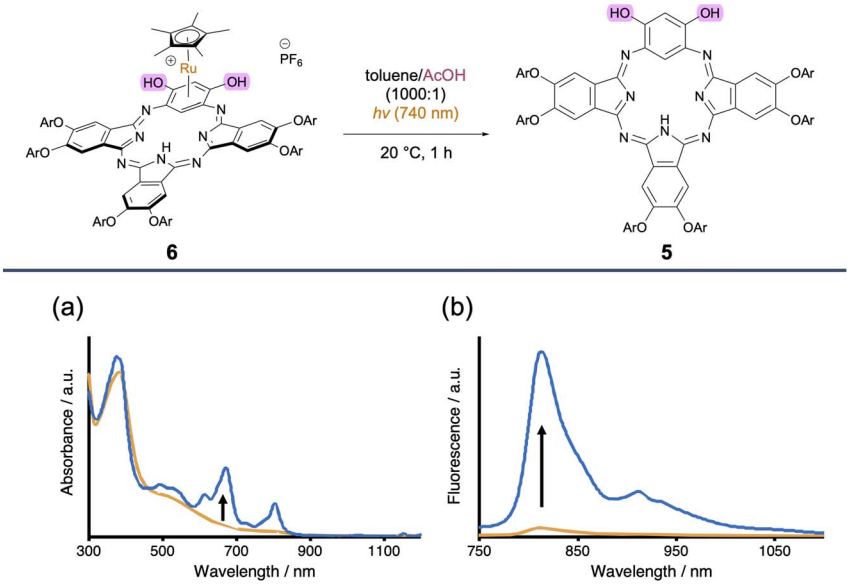

Fig. 7 OFF/ON NIR activation of **6** by NIR irradiation. (a) Electronic absorption spectra and (b) emission spectra (λ_{ex} = 500 nm) of **6** before (orange) and after (blue) NIR irradiation, measured in toluene/AcOH (1000 : 1).

result seems counterintuitive, considering that Ru π-phenol complexes are typically more stable than Ru π-benzene complexes, since electron-rich arenes stabilize electron-deficient metal centers.[22] Therefore, the observed difference in stability between **3** and **4** can be ascribed to the phenol–quinoid tautomerism within the BPc framework, reflecting a contrast between the 6π local and 18π global (macrocyclic) aromaticity. Ru π-naphthalene complexes are known to be more labile than Ru π-benzene complexes due to the delocalized nature of intrinsic 10π aromatic systems.[22] Similarly, Ru-BPc complex **4**, which contains a hydroxy group, partially adopts a resonance structure with global 18π aromaticity at the cost of local 6π aromaticity in the benzene ring. This resonance leads to weaker η^6-coordination of Ru to the arene, although the contribution is not large (Fig. 4b). In contrast, compound **3**, which lacks the hydroxy functionality, cannot attain the global 18π aromatic quinoid form, and remains fixed in the locally 6π aromatic benzene structure. Therefore, the dissociation appears to be driven by the contribution of the globally 18π aromatic system in BPc.

We speculated that this NIR-responsive photodissociation of Ru-BPcs could enable an OFF/ON NIR activation system, in which a weakly NIR-absorptive precursor is converted into a strongly NIR-absorptive/emissive state by NIR light. Although ON/OFF NIR switching has been reported,[9,11] and leuco-type methylene blue derivatives have recently shown OFF/ON behavior in the far-red region (600–700 nm),[17,55,56] OFF/ON systems operating in the NIR range remain elusive. We focused on dihydroxy BPc **5**, which exhibits strong absorption and fluorescence in the NIR region due to a significant contribution of the quinoid form resulting from the electron-rich resorcinol unit.[27,29] Therefore, its Ru complex **6** was expected to show a large change in NIR optical properties upon demetallation. **6** was synthesized similarly to **3** and **4** (see SI). As expected, Ru complexation significantly weakened the 18π-aromaticity. The changes in NIR properties accompanying photochemical release of Ru from **6** to **5** were investigated in toluene/AcOH (1000 : 1) (Fig. 7). **6** exhibited weak, broad absorption in the NIR region. The faint emission of **6** is attributable to trace amounts of **5**, generated by irradiation during the fluorescence measurement. After NIR irradiation, these spectra were altered significantly with the generation of **5**. NIR absorption peaks appeared at 671 nm and 804 nm, and the emission maximum at 814 nm increased significantly. This result highlights the potential applicability of our Cp*Ru-BPc system for NIR-responsive OFF/ON activatable system, which is potentially useful for phototheranostics that enables simultaneous fluorescence imaging, photodynamic therapy, and chemotherapy.[57]

Conclusions

We have designed, synthesized, and characterized a series of Cp*Ru-BPc π-complexes with intrinsic 6π/18π aromaticity. The complexation of BPcs with the Cp*Ru unit proceeded selectively at the benzene moiety, as confirmed by X-ray crystallography and NMR spectroscopy. The coordination of Ru to BPcs shifts the phenol–quinoid tautomerism towards the phenol form, weakening the 18π aromaticity and NIR absorption. However, the Ru-BPc complexes exhibit S_0–T_1 absorption in the NIR region, and this can be utilized to enable NIR-responsive Ru-uncaging reactions of hydroxy-substituted BPc complexes. This NIR photodissociation reaction modulates the NIR optical properties, affording a groundbreaking OFF/ON NIR activatable system. Our characterization of this NIR-responsive aromaticity-driven Ru π-complex photochemistry based on low-energy S–T transition provides new molecular and mechanistic insights into the design of Ru-photoresponsive systems operating in the

deeper NIR region, with excitation wavelengths of up to 850 nm, substantially exceeding those of previously reported Ru-based photocages. Notably, the OFF/ON-type NIR fluorescence change upon Ru photo-uncaging provides an intrinsic fluorescence response that enables spatiotemporal tracking of metal release without the need for any external probe. To our knowledge, this dual functionality has no precedent among reported Ru-based photocage systems. We believe our characterization of this system provides a fundamental basis for future developmental research, opening up new possibilities for optoelectronic and biomedical applications, for example in phototheranostics, where it could enable site-selective chemotherapy *via* Ru release and simultaneous NIR fluorescence imaging of the release sites.

Author contributions

Conceptualization: N. T., M. U. methodology: O. T., N. T., M. U. investigation: O. T., N. T. supervision: N. T., M. U. writing – original draft: O. T., N. T. Writing – review & editing: O. T., N. T., K. H., M. U.

Conflicts of interest

The authors declare no competing interests.

Data availability

CCDC 2472097 and 2472098 contain the supplementary crystallographic data for this paper.[58a,b]

The data supporting the findings of this article are available within the paper and its supplementary information (SI). Supplementary information: experimental procedures, computational data, and characterization data. See DOI: https://doi.org/10.1039/d5sc09646d.

Acknowledgements

This work was supported in part by grants from JSPS KAKENHI (A) (No. 22H00320, 25H00875), JSPS KAKENHI Transformative Research Areas (A) (No. 22H05125), JST CREST (No. JPMJCR19R2), Asahi Glass Foundation, NAGASE Science Technology Foundation, Naito Foundation, Chugai Foundation, Uehara Memorial Foundation (to M. U.), JSPS KAKENHI for Young Scientists (No. 22K15245), JSPS KAKENHI (B) (No. 24K02142), JST FOREST (No. JPMJFR240E), Asahi Glass Foundation, Naito Foundation, Mochida Memorial Foundation, Uehara Memorial Foundation (to N. T.), JSPS KAKENHI for Research Activity Start-up (No. 25K23780), and JST SPRING (No. JPMJSP2108) (to O.T.).

References

1 J. Fabian, H. Nakazumi and M. Matsuoka, *Chem. Rev.*, 1992, **92**, 1197–1226.
2 G. Qian and Z. Y. Wang, *Chem.–Asian J.*, 2010, **5**, 1006–1029.
3 G. Hong, A. L. Antaris and H. Dai, *Nat. Biomed. Eng.*, 2017, **1**, 0010.
4 A. Abdollahi, H. Roghani-Mamaqani, B. Razavi and M. Salami-Kalajahi, *ACS Nano*, 2020, **14**, 14417–14492.
5 D. Meng, R. Zheng, Y. Zhao, E. Zhang, L. Dou and Y. Yang, *Adv. Mater.*, 2022, **34**, 2107330.
6 Y. Chen, S. Wang and F. Zhang, *Nat. Rev. Bioeng.*, 2023, **1**, 60–78.
7 Z.-H. Wu, M. Peng, C. Ji, P. Kardasis, I. Tzourtzouklis, M. Baumgarten, H. Wu, T. Basché, G. Floudas, M. Yin and K. Müllen, *J. Am. Chem. Soc.*, 2023, **145**, 26487–26493.
8 S. Jia and E. M. Sletten, *ACS Chem. Biol.*, 2022, **17**, 3255–3269.
9 Z. Zhang, W. Wang, M. O'Hagan, J. Dai, J. Zhang and H. Tian, *Angew. Chem., Int. Ed.*, 2022, **61**, e202205758.
10 Y. Fu, N. A. Simeth, W. Szymanski and B. L. Feringa, *Nat. Rev. Chem.*, 2024, **8**, 665–685.
11 Y. Xu, Y. Tang and Q. Li, *Adv. Funct. Mater.*, 2025, **35**, 2416359.
12 P. Lentes, E. Stadler, F. Röhricht, A. Brahms, J. Gröbner, F. D. Sönnichsen, G. Gescheidt and R. Herges, *J. Am. Chem. Soc.*, 2019, **141**, 13592–13600.
13 L. Köttner, E. Ciekalski and H. Dube, *Angew. Chem., Int. Ed.*, 2023, **62**, e202312955.
14 P. Shrestha, D. Kand, R. Weinstain and A. H. Winter, *J. Am. Chem. Soc.*, 2023, **145**, 17497–17514.
15 Z. Li, X. Ma, J. Song, Q. Wang, Y. Feng, H. Liu, P. Zhang, H. Guo and J. Yin, *Chem. Sci.*, 2025, **16**, 1762–1771.
16 K. Satake, N. Ootsuki, K. Higashiguchi and K. Matsuda, *J. Am. Chem. Soc.*, 2025, **147**, 9653–9664.
17 Q. Hu, J. Du, S. A. A. Abedi, X. Liu, S. Long, W. Sun, J. Fan and X. Peng, *Angew. Chem., Int. Ed.*, 2025, **64**, e202504670.
18 T. P. Gill and K. R. Mann, *Organometallics*, 1982, **1**, 485–488.
19 A. M. McNair, J. L. Schrenk and K. R. Mann, *Inorg. Chem.*, 1984, **23**, 2633–2640.
20 J. L. Schrenk, A. M. McNair, F. B. McCormick and K. R. Mann, *Inorg. Chem.*, 1986, **25**, 3501–3504.
21 K. R. Mann, A. M. Blough, J. L. Schrenk, R. S. Koefod, D. A. Freedman and J. R. Matachek, *Pure Appl. Chem.*, 1995, **67**, 95–101.
22 N. V. Shvydkiy and D. S. Perekalin, *Coord. Chem. Rev.*, 2020, **411**, 213238.
23 A. W. Kelly and K. T. Holman, *Angew. Chem., Int. Ed.*, 2022, **61**, e202115556.
24 B. Akana-Schneider, Y. Guo, B. Parnitzke and J. Derosa, *Dalton Trans.*, 2024, **53**, 18819–18827.
25 J. A. Elvidge and J. H. Golden, *J. Chem. Soc.*, 1957, 700–709.
26 A. Çetin, S. Sripothongnak, M. Kawa, W. S. Durfee and C. J. Ziegler, *Chem. Commun.*, 2007, **43**, 4289–4290.
27 N. Toriumi, A. Muranaka, K. Hirano, K. Yoshida, D. Hashizume and M. Uchiyama, *Angew. Chem., Int. Ed.*, 2014, **53**, 7814–7818.
28 N. Toriumi, A. Muranaka, D. Hashizume and M. Uchiyama, *Tetrahedron Lett.*, 2017, **58**, 2267–2271.
29 N. Toriumi, N. Asano, T. Ikeno, A. Muranaka, K. Hanaoka, Y. Urano and M. Uchiyama, *Angew. Chem., Int. Ed.*, 2019, **58**, 7788–7791.

30 N. Toriumi, A. Muranaka and M. Uchiyama, *Chem. Pharm. Bull.*, 2023, **71**, 462–465.
31 S. Yanagi, A. Matsumoto, N. Toriumi, Y. Tanaka, K. Miyamoto, A. Muranaka and M. Uchiyama, *Angew. Chem., Int. Ed.*, 2023, **62**, e202218358.
32 S. Yanagi, O. Takayama, N. Toriumi, A. Muranaka, D. Hashizume and M. Uchiyama, *Chem.–Eur. J.*, 2024, **30**, e202400401.
33 K. K. Dailey, G. P. A. Yap, A. L. Rheingold and T. B. Rauchfuss, *Angew. Chem., Int. Ed.*, 1996, **35**, 1833–1835.
34 S. M. Contakes, S. T. Beatty, K. K. Dailey, T. B. Rauchfuss and D. Fenske, *Organometallics*, 2000, **19**, 4767–4774.
35 L. Cuesta and J. L. Sessler, *Chem. Soc. Rev.*, 2009, **38**, 2716–2729.
36 L. Cuesta, E. Karnas, V. M. Lynch, P. Chen, J. Shen, K. M. Kadish, K. Ohkubo, S. Fukuzumi and J. L. Sessler, *J. Am. Chem. Soc.*, 2009, **131**, 13538–13547.
37 E. Caballero, J. Fernández-Ariza, V. M. Lynch, C. Romero-Nieto, M. S. Rodríguez-Morgade, J. L. Sessler, D. M. Guldi and T. Torres, *Angew. Chem., Int. Ed.*, 2012, **51**, 11337–11342.
38 I. Grocka, L. Latos-Grażyński and M. Stępień, *Angew. Chem., Int. Ed.*, 2013, **52**, 1044–1048.
39 A. Nakai, S. Ishida, T. Soya and A. Osuka, *Angew. Chem., Int. Ed.*, 2019, **58**, 8197–8200.
40 A. Nakai, T. Tanaka and A. Osuka, *Molecules*, 2020, **25**, 2753.
41 A. Igau, *Coord. Chem. Rev.*, 2017, **344**, 299–322.
42 T. Schulte, Z. Wang, C.-C. Li, A. Hamad, F. Waldbach, J. Pampel, R. Petzold, M. Leutzsch, F. Bahns and T. Ritter, *J. Am. Chem. Soc.*, 2024, **146**, 15825–15832.
43 K. Chen, Y. Ma, Y. Lin, J.-Y. Li and H. Shi, *J. Am. Chem. Soc.*, 2024, **146**, 15833–15842.
44 P. S. Pregosin, *NMR in Organometallic Chemistry*, Wiley-VCH, Weinheim, 2013.
45 T. Kinoshita, J. T. Dy, S. Uchida, T. Kubo and H. Segawa, *Nat. Photonics*, 2013, **7**, 535–539.
46 S. Amemori, Y. Sasaki, N. Yanai and N. Kimizuka, *J. Am. Chem. Soc.*, 2016, **138**, 8702–8705.
47 T. Kinoshita, *Bull. Chem. Soc. Jpn.*, 2022, **95**, 341–352.
48 J. Michl, *J. Am. Chem. Soc.*, 1978, **100**, 6819–6824.
49 M. Wang and K. Ishii, *Coord. Chem. Rev.*, 2022, **468**, 214626.
50 T. G. Traylor, K. Stewart and M. Goldberg, *J. Am. Chem. Soc.*, 1984, **106**, 4445–4454.
51 S. Bonnet, *J. Am. Chem. Soc.*, 2023, **145**, 23397–23415.
52 L. M. Loftus, K. F. Al-Afyouni and C. Turro, *Chem.–Eur. J.*, 2018, **24**, 11550–11553.
53 M. H. Al-Afyouni, T. N. Rohrabaugh, K. F. Al-Afyouni and C. Turro, *Chem. Sci.*, 2018, **9**, 6711–6720.
54 Y. Husiev, S. K. Götzfried, M. L. A. Hakkennes, D. Kotova, I. T. Nolthenius, C. van de Griend, A. C. Johns, S. Abyar, M. A. Siegler, A. Kornienko and S. Bonnet, *J. Am. Chem. Soc.*, 2025, **147**, 44356–44371.
55 H. M. Dao, C.-H. Whang, V. K. Shankar, Y.-H. Wang, I. A. Khan, L. A. Walker, I. Husain, S. I. Khan, S. N. Murthy and S. Jo, *Chem. Commun.*, 2020, **56**, 1673–1676.
56 Y. Zhang, P. Zhao, X. Chen, C. Xu, J. Guo, X. Qu, X. Hu, H. Gao, P. Huang and J. Zhang, *ACS Appl. Mater. Interfaces*, 2023, **15**, 12750–12765.
57 W. Hu, P. N. Prasad and W. Huang, *Acc. Chem. Res.*, 2021, **54**, 697–706.
58 (*a*) CCDC2472097: Experimental Crystal Structure Determination, 2026, DOI: 10.5517/ccdc.csd.cc2nzf25; (*b*) CCDC2472098: Experimental Crystal Structure Determination, 2026, DOI: 10.5517/ccdc.csd.cc2nzf36.